Topology and Polarity of Dislocation Cores Dictate the Mechanical Strength of Monolayer MoS₂

Jianyang Wu,[1, 2,*] Zhisen Zhang,[1] Jianying He[2], Pilar Ariza[3], Michael Ortiz[4] and Zhiliang Zhang [2,*]

[1]Department of Physics, Research Institute for Biomimetics and Soft Matter, Jiujiang Research

Institute and Fujian Provincial Key Laboratory for Soft Functional Materials Research, Xiamen University, Xiamen 361005, PR China

[2]NTNU Nanomechanical Lab, Norwegian University of Science and Technology (NTNU), Trondheim 7491, Norway

[3]Escuela Técnica Superior de Ingeniería, Universidad de Sevilla, Camino de los descubrimientos, s.n., 41092, Sevilla, Spain

[4]Division of Engineering and Applied Science, California Institute of Technology, CA, 91125, Pasadena, USA

Abstract: In contrast to homoelemental graphene showing common dislocation dipole with pentagon-heptagon (5|7) core, heteroelemental MoS₂ is observed to contain diverse dislocation cores that tune the chemical and physical properties. Yet, how the inevitable dislocation cores in MoS₂ affect the mechanical behaviours remains virtually unexplored. Herein, we report direct atomistic simulations of mechanical characteristics of isolated dislocation-embedded MoS₂ monolayers under tensile load. All isolated dislocation cores in MoS₂ monolayer rise polar stress-concentration, while those with larger Burgers vector are less energetically-favorable configurations but show local wrinkling behaviour. It is revealed that the intrinsic tensile strength of MoS₂ is dictated by topology and polarity of dislocation cores. There is a strong inverse correlation between the maximum residual stresses induced by the dislocation cores and the strength of MoS₂ monolayers. Mechanical failure initiates from the bond at dislocation polygon on which side there is a missing atomic chain. Armchair-oriented 4|8 dislocation exhibits sole brittle failure, however, dual brittle/ductile fractures occur in zigzag-oriented dislocations; Mo-S-Mo angle-oriented crack is brittle, while the S-Mo-S angle-oriented crack becomes ductile. Our findings shed sights on mechanical design of heteroelemental 2D materials via dislocation engineering for practical application.

*Corresponding authors: jianyang@xmu.edu.cn, zhiliang.zhang@ntnu.no

Keywords: monolayer MoS_2, dislocation cores, molecular dynamics simulations, mechanical strength, fracture characteristics

Highlights

- The presence of single dislocation cores alters the structural characteristics and rises polar stress-concentration in monolayer molybdenum disulfide

- Mechanical strength of monolayer molybdenum disulfide is dictated by the topology and polarity of dislocation cores

- Dual brittle/ductile fracture characteristics occur monolayer molybdenum disulfide depending on the angular failure orientation

1. Introduction

Two-dimensional (2D) crystalline structures, such as graphene, hexagonal boron nitride (*h*-BN), silicene, phosphorene and transition metal-dichalcogenides (TMDCs, for example MoS_2), have become a major research interest in fundamental science and potential technological applications in recent years [1, 2]. The diverse families of 2D structures collectively cover not only a full spectrum of physical behaviours, for example, from conducting graphene to semiconducting MoS_2 and to insulating *h*-BN, but also a unique combination of mechanical properties, with high in-plane strength and stiffness yet low out-of-plane stiffness [3, 4].

As one of the most captivating and fundamental concepts in materials science, dislocations are ubiquitous defects existing in real crystalline solids fabricated under a variety of laboratory-settings [1, 2]. In relatively simple 2D graphene, pentagon-heptagon (5|7) edge dislocation predominates due to its lower strain energy than other polygonal dislocations, for example, energy-unfavourable square-octagon (4|8) dislocation. The 5|7 dislocation is able to occur in pairs in crystalline domains

under certain conditions. As an example, under electron beam irradiation, 90°rotation of a C-C bond of hexagonal ring in pristine lattice domains results in formation of two antiparallel edge dislocations with 5|7 cores, termed as Stone-Wales defects (SWDs)[5-7]. Once a sufficient shear stress is imposed to the SWD-embedded crystals, its two-component 5|7 dislocations split apart [7, 8].

From a topological perspective, three-atomic-layer MoS_2 lattice shows more rich variety of concave dreidel-shaped dislocation cores such as 5|7, 6|8, 4|4, 4|6 and 4|8 structural motifs [9-14], in contrast to monatomic graphene showing the most common 5|7 dislocation [15-19]. Moreover, because of the structural heterogeneity, MoS_2 produced by chemical-vapor-deposition (CVD) shows elemental polarity in the growth fronts, with either Mo or S terminated edges, which can result in Mo- or S-oriented polar dislocation, as well as different topological dislocations that have identical elemental compositions. For example, a polar Mo-oriented 5|7 dislocation (Mo5|7) core composed of 5Mo+10S atoms is structurally characterized by 2Mo atoms forming a Mo-Mo homoelemental bond that separates the 5- and 7-fold rings, whereas for a S-oriented counterpart (S5|7) is identified by 4S atoms constituting double S-S homoelemental bonds shared by the 5- and 7-fold rings. Also, unlike graphene, SWDs formed by rotation of polar bonds is not expected in bielemental hexagonal MoS_2 because of the polar nature of its chemical bonds and the trigonal symmetry. However, in analogous to graphene, migration of dislocations was also identified in TMDCs both experimentally and theoretically [20-24].

The diverse set of structural dislocations in MoS_2 opens exciting opportunities for tailoring its properties or even creating new functionalities. For instance, 5|7 dislocations are ferromagnetic, showing transition from semiconductor to half-metal and to metal depending on the density of dislocations, while 4|8 dislocations can be antiferromagnetic semiconductor [14, 25]. Moreover, a 4|4 dislocation-dominated grain boundary (GB) exhibits perfect metallicity [10]. Depending on the topology and arrangement of dislocations, dislocations-dominated GBs enable large variations in

band gap and electrical conductivity, enhancement or quenching in photoluminescence, and other properties [11, 12, 25-31].

Given the fact that dislocations are unavoidable in MoS_2 but play a critical role in altering the physical properties in various ways, understanding how dislocations affect the fundamental mechanical properties of this material is of critical importance for the design of MoS_2-based devices. To date, there is no studies on the role of dislocations on the mechanical properties and failure mechanisms of MoS_2, although there is a good understanding on how the predominant 5|7 dislocations influence the morphological and mechanical properties of graphene [1, 3, 32-38]. To this end, the intrinsic strengths and failure behaviours of monolayer MoS_2 containing distinctly representative dislocation cores subjected to uniaxial tension are systematically explored by atomistic simulations. The results show that the intrinsic strengths of MoS_2 are critically dependent on both the topology and polarity of dislocation cores, and the failure behaviours are dictated by the orientation of polar dislocations.

2. Simulation Methods

The mechanical properties of monolayer MoS_2 containing an isolated dislocation was investigated by molecular dynamics (MD) simulations using the LAMMPS package. To prevent finite-size effects, sheets with planar dimensions of approximately 450×450 $Å^2$ were generated. A modified MoS_2-type Reactive Empirical Bond-Order (REBO) potential that has been successfully applied to predict the mechanical characteristics of MoS_2 [22, 39-42] was employed to describe the atomic interactions in the systems. Dislocation-embedded MoS_2 were initially relaxed with a sufficient simulation time of 30 ps for mechanical tests. As-equilibrated samples were then deformed with a constant strain-rate of 1.0×10^8/s under uniaxial tension along one the X direction that is perpendicular to the isolated dislocation in MoS_2 monolayers. The velocity-Verlet method with a small timestep of 0.1 fs was utilized to integrate the equation of atomic motions. To ensure a regime of localized deformation

despite the high strain-rate utilized, the tension simulations were performed at a low-temperature of 10 K. Periodic boundary conditions (PBC) were only applied along one planar X direction, while the free PBC were used along the other planar and off-plane directions, corresponding to Y- and Z-axis, respectively. These boundary conditions allow the sheet to contract freely due to the Poisson effect. Atomic stress tensor of Mo and S atoms in the system was calculated on the basis of virial stress definition and the thickness of the MoS_2 monolayer was assumed to be 6.5 Å for determining the atomic stresses [43].

3. Results and discussion

3.1 Diverse dislocation cores in MoS_2 monolayers

Because monolayer MoS_2 sheet is isomorphic to graphene from the off-plane view, an isolated dislocation core in MoS_2 can be constructed by removing a semi-infinite strip with width of Burgers vector $\left|\vec{b}_{(1,0)}\right|$, $\left|\vec{b}_{(1,0)+(1,0)}\right|$ or $\left|\vec{b}_{(1,1)}\right|$ along armchair or zigzag direction from an otherwise 2D monocrystal, and by reconnecting all of the resulting dangling bonds seamlessly, as shown in Fig. 1. Dislocation-embedded MoS_2 sheet shows localized lattice distortion in the vicinity of the dislocation core, in contrast to perfect pristine MoS_2 (Figs. 1a and b). Because of the trigonal symmetry, cutting out half of an armchair atomic row from S to Mo direction results in Mo-oriented polar dislocations including Mo5|7, Mo6|8 and Mo4|6 topological motifs (Figs. 1d-f). Inversely, S-oriented polar counterparts including S5|7, S6|8 and S4|6 cores are yielded (Figs. 1i-k). Both Mo5|7 and S5|7 dislocation cores show energetically unfavourable Mo-Mo and S-S homoelemental bonds in the center of dislocations, respectively. For 6|8 edge dislocations, there exists either coordinatively unsaturated single Mo-atom or double S-atoms in the center. However, Mo- and S-atoms in the center of 4|6 dislocations show 8- and 4-fold coordination, respectively. At the atomic level, both 6|8 and 4|6 dislocations can be derived from the common 5|7 dislocations by inserting or removing single Mo-atom or double S-atoms in the center of the dislocation core. For instance, embedment of one Mo-atom in the center of

S5|7 dislocation yields S6|8 dislocation. Unlike aforementioned dislocations, more complex 4|4|6 and 6|7|8 dislocation structures are accomplished by removing two parallel halves of an armchair atomic chain on one side (Figs. 1g, h, l and m). These dislocations possesses identical 2-folds large Burgers vector $\left|\vec{b}_{(1,0)+(1,0)}\right|$. 8- and 4-fold coordination of Mo- and S-atoms in the center of 4|4|6 dislocations are presented, whereas for the 6|7|8 dislocations either 2 Mo- or 4 S-atoms are coordinatively unsaturated. Those dislocations show left-right mirror symmetry. Notably, a dislocation with 4|8 core is created by removing two parallel zigzag atomic chains and is homoelemental bonds-free. However, this edge dislocation shows a $\sqrt{3}$-folds large Burgers vector $\left|\vec{b}_{(1,1)}\right|$ and broken left-right mirror symmetry. All the atoms in this dislocation are coordinatively preserved.

3.2 Energetics of dislocation cores

The stability of those dislocation cores can be compared by the total potential energy calculation. Due to the polarity and logarithmic divergence in the far-field elastic contribution [9], however, the magnitude of the absolute energy of an isolated dislocation in MoS$_2$ monolayer is difficult to be determined accurately. Here, the total relative potential energies of single dislocation cores with respect to the pristine crystal are evaluated as

$$\Delta E = \sum_{i}^{n} e_{\mathrm{Mo}}^{\mathrm{dis}} + \sum_{j}^{m} e_{\mathrm{S}}^{\mathrm{dis}} - n e_{\mathrm{Mo}}^{\mathrm{bulk}} - m e_{\mathrm{S}}^{\mathrm{bulk}} \tag{1}$$

where $e_{\mathrm{Mo}}^{\mathrm{dis}}$, $e_{\mathrm{S}}^{\mathrm{dis}}$ and $e_{\mathrm{Mo}}^{\mathrm{bulk}}$, $e_{\mathrm{S}}^{\mathrm{bulk}}$ are the Mo- and S-atomic potential energies of dislocation cores and perfect MoS$_2$ lattice, respectively. n and m are the number of Mo and S atoms in single dislocations, respectively. It is noted that wrinkles induced by a single dislocation with large Burgers vectors are not allowed in MoS$_2$ monolayers when the atomic potential energies were calculated. Fig. 2a shows the calculated ΔE for the 11 dislocation cores. As is expected, single 4|4|6 and 6|7|8 dislocations with larger Burgers vector exhibit higher ΔE, indicating their less energetically-

favourable structures. Armchair-oriented 4|8 dislocation with similar larger Burgers vector yields a lower ΔE than those of single 4|4|6 and 6|7|8 dislocations, implying its higher stability. However, zigzag-oriented dislocations with smaller Burgers vector show low values of ΔE ranging from around 3.5-6.0 eV, which are similar to that single 5|7 dislocation in graphene (about 5.0 eV) [44], and thus are relatively energetically-favourable lattice defects. Remarkably, Mo5|7, Mo6|8 and S6|8 dislocations with higher ΔE arise from the existence of coordinatively unsaturated Mo, Mo and S atoms in the central of dislocation cores, respectively. Overall, the stability of isolated dislocations in MoS$_2$ monolayer is critically dependent on both the topology and chemical compositions. Moreover, dislocations cause changes in atomic potential energies of surrounding perfect hexagons in MoS$_2$ monolayers (Fig. S1). However, it should be also mentioned that the thermodynamic stability of specific dislocation structure changes depending on factual conditions.

3.3 Bond characteristics in single dislocation-contained MoS$_2$ monolayers

Those dislocations in covalent MoS$_2$ lattices could introduce remarkable levels of bond and angle deformations. Lattice distortion is analysed by measuring bond angles of S-Mo-S and Mo-S-Mo in central dislocation-contained nanoribbon, as plotted in Fig. 2b. For both Mo5|7 and S5|7 dislocation-embedded lattices, the largest bond angles locate at the heptagon, while the smallest bond angles correspond to the pentagon. Slight difference in bond angles at the heptagon-pentagon dipoles between the two polar dislocations indicates the disparity in the geometry of their cluster motifs. This arises from the different orientations in distinct hetero- and homo-elemental bonds, with polar Mo-S connecting sandwich layers, S-S in the surface layers and Mo-Mo in the central layer. The amplitudes of bond angles decreases away from the dislocation cores and far-field distributions of bond angles are renormalized to decay. However, due to the presence of one extra armchair atomic chain, far-field bond angles on the heptagon side are higher than those on the pentagon side. Bond analysis shows an inhomogeneous field of bond strain around the misfit dislocation cores as shown

in Fig. 2c. The atomic level strains (Δl) in single dislocation-contained MoS$_2$ monolayers are defined

by the relative change of the bond lengths with respect to perfect MoS$_2$ as

$$\Delta l = \frac{l_{\text{disl}} - l_{\text{bulk}}}{l_{\text{bulk}}} \qquad (2)$$

where l_{disl} and l_{bulk} are the bond lengths in the lattices with an edge dislocation and dislocation-free,

respectively. For all studied defective MoS$_2$ structures, strong strain field situates at the immediate

dislocation core zone. Within the upper half-region, the strains are positive and tensile due to

deficiency of atomic chains, whereas within the lower half-region the strains are negative and

compressive. Both tensile and compression strains fade out from the dislocation cores. For a given

ring, however, the bonds forming small angles to the vertical direction are less strained. In

comparison, lattices containing 4|8, 4|4|6 and 6|7|8 dislocations with large Burgers vector are more

locally strained than those with 5|7, 6|8 and 4|6 dislocations. For dislocations showing similar

topology, there is no significant difference in bond strains.

3.4 Pre-stress in single dislocation-embedded MoS$_2$ monolayers

The pre-stress field induced by an edge dislocation in thin membrane from the 2D elastic theory is

expressed by [34, 38, 45]

$$\sigma_{xx} = -Dy\frac{3x^2 + y^2}{(x^2 + y^2)^2}, \ \sigma_{yy} = Dy\frac{x^2 - y^2}{(x^2 + y^2)^2} \ \text{and} \ \sigma_{xy} = -Dx\frac{x^2 - y^2}{(x^2 + y^2)^2} \qquad (3)$$

where $\sigma_{\alpha\beta}$ ($\alpha\beta = x, y$) are the in-plane stress components for dislocation-contained lattices, and D

is a pre-factor determining the amplitude of residual stresses. Here the parameter D is set to be -35

N/m for the MoS$_2$ monolayer. The in-plane stress contours of isolated Mo5|7 dislocation in

freestanding monolayer MoS$_2$ from both MD simulations and 2D elastic theory are shown in Figs.

3a-c and S2. As is expected, both MD simulations and theory predict heterogeneous atomic-level

in-plane stresses around the dislocation, with the maximum and minimum stresses located at the heptagonal and pentagonal rings, respectively. Similar to the case in 2D graphene [46], dipolar stress fields in σ_{xx} and principal stress $\sigma_p = (\sigma_{xx} + \sigma_{yy})/2$ are identified due to an isolated dislocation in the hexagonal lattice. Left-right mirror symmetry in the in-plane stresses of σ_{xx}, σ_{yy} and $\sigma_p = (\sigma_{xx} + \sigma_{yy})/2$ is identified. However, the theoretical solution predicts perfect up-down 'inversion' symmetry in in-plane stresses of σ_{xx}, σ_{yy} and $\sigma_p = (\sigma_{xx} + \sigma_{yy})/2$, in contrast to the MD results. Although both S-layers and the Mo-layer show dipolar stress fields from MD simulation, the magnitude in localized stresses are different. The magnitude of both the maximum and minimum in-plane stresses in Mo-layer is pronouncedly larger than those in S-layers. Remarkably, higher σ_{xx} on the heptagon side in the Mo-layer than in both S-layers suggests that Mo-layer are more pre-stressed in tension, however, the zone of pentagon side in the top-bottom S-layers are more pre-stressed in compression. The flexible coordination number of S-atom mainly explains the different pre-stress scenarios from that of Mo-atoms. For shear stress component σ_{xy}, the up-down 'inversion' symmetry in the stress contour plots predicted by MD simulation are nearly identical to its theoretical counterpart. For MoS$_2$ lattice containing other topological dislocations, similar scenarios in in-plane stress contours are identified.

3.5 Dislocation-induced wrinkles in MoS$_2$ monolayers

 As opposed to truly 2D graphene which shows low flexural rigidity, tri-atomic-layered MoS$_2$ exhibits much higher flexural rigidity and are thus difficult to wrinkle [47]. Beyond the in-plane geometrical distortion, topological defects such as disclinations and dislocation in 2D structures also causes rough surface morphology away from planarity. Fig. 4 shows the morphological configurations of isolated dislocation-contained MoS$_2$ monolayers. Interestingly, MoS$_2$ monolayers containing single isolated 5|7, 4|6 and 6|8 dislocations are non-wrinkled near the dislocations, in

sharp contrast to graphene. This reflects its high flexural rigidity over graphene. However, MoS_2 lattices with 4|8, 4|4|6 or 6|7|8 dislocations that have larger Burgers vectors, around $\left|\vec{b}\right|^2 = 3$ folds higher than other topological dislocations, tend to undergo out-of-plane displacements for effectively relieving the in-plane strain energy triggered by the dislocation cores. The mechanism of dislocation-induced vertical deformation is similar to the case of monatomic graphene [3, 33, 35, 36, 45, 46, 48]. Nevertheless, the amplitude of dislocation-induced wrinkles in MoS_2 monolayers is larger than that in graphene. Moreover, those dislocation cores are locally self-bend-deformed for achieving the curved wrinkles, and S4|4|6 dislocations is able to self-reconstruct, forming fresh dislocation-based cluster (Fig. S3). It is also observed that the pre-stress fields in those dislocation-embedded MoS_2 with and without off-plane rippling deviate pronouncedly in magnitude, shape and distribution. For example, due to the off-plane deformation, significant reduction in the zone of amplified stress around the dislocation core occurs, and the stress contour plots becomes asymmetric.

3.6 Mechanical properties of single dislocation-embedded MoS_2 monolayers

Such variations in structural characteristics and pre-stress fields of MoS_2 by dislocation defects would impact its mechanical properties. Figs. 5a-d presents the mechanical stress-strain curves and the tensile strengths of various dislocation-contained monolayer MoS_2 under uniaxial straining, respectively. Mechanical responses of pristine MoS_2 are shown in Fig. 4S for comparison. Defect-free MoS_2 yields uniaxial tensile modulus of 159.0 and 157.7 GPa and uniaxial fracture strength of 27.0 and 26.3 GPa for the armchair and zigzag directions (Fig. S4), respectively, in agreement with previous first-principle calculations [40, 41]. In comparison, as is expected, both dislocation-contained and -free MoS_2 yield remarkable disparity in mechanical responses. The presence of isolated dislocation in MoS_2 leads to significant degradation in the mechanical properties, for example, with the minimum loss by about 40% in strength. However, there are significant

differences in the mechanical responses among MoS_2 layers including different dislocations. For the case with Mo-oriented polar dislocations, the tensile strength greatly depends on the topology of the dislocation, and it can be sorted as Mo5|7 > Mo4|6 > Mo6|8 > Mo6|7|8 > Mo4|4|6. Lattice with Mo5|7 isolated dislocation shows over 27.5% higher strength than that with derivative Mo4|6 or Mo6|8 dislocation, although Mo5|7, Mo4|6 and Mo6|8 dislocations exhibit similar intrinsic in-plane strain energy because of their equivalent small Burgers vector $\left|\vec{b}_{(1,0)}\right|$. Comprehensibly, Mo6|7|8 or Mo4|4|6 contained-lattice is mechanically weakened due to high intrinsic strain energy. Specifically, two sudden drops in strength of Mo4|4|6-contained lattice indicate break-vs-arrest behaviour during deformation. For S-oriented polar dislocations, however, in terms of tensile strength, they are ranked as S4|6 > S5|7 > S6|8 > S6|7|8 > S4|4|6. This indicates that the S4|6 dislocation is more stable than the S5|7, differing from the case of Mo-oriented polar dislocations. This is also confirmed by previous first-principle calculations revealing that 5|7 dislocation in an S-polar GB energetically favourably transforms to S4|6 dislocation [49]. In comparison, the difference in strength between S5|7, S4|6 and S6|8 dislocation contained lattices is not significant as for Mo-oriented polar dislocation embedded-ones. For a given topology of dislocation, lattice with S-oriented polar dislocation is mechanically robust than that with Mo-oriented polar one. This is because the coordination number of S-atom is more flexible than that of Mo atom and the Mo-ligand bonds are relatively weak. For the armchair-oriented 4|8 dislocation, the strength is lower than those of 5|7, 4|6 and 6|8 dislocations, yet comparable to those of 4|4|6 and 6|7|8 dislocations. Similar to graphene, intrinsic wrinkles in lattice by 4|8 or 4|4|6 or 6|7|8 dislocations can be effectively suppressed by imposing tensile strain. The maximum residual *von Mises* stresses σ_{von} in isolated dislocation-contained lattices are shown in Fig. 5e. The maximum σ_{von} appears in the bonds located at the dislocation cores. Apparently, for both Mo- and S-oriented dislocation-contained lattices, it is

revealed that the failure strength is inversely correlated with the maximum residual σ_{von}. The results reveal that the strength of MoS$_2$ is dictated by both the topology and polarity of dislocations.

3.7 Dual brittle/ductile fractures in MoS$_2$ monolayers

To further explore fracture mechanisms in the MoS$_2$ layers, the development of molecular structures of dislocation-embedded MoS$_2$ under uniaxial tension is explored. As an example, the deformation failure processes of Mo5|7 dislocation-contained MoS$_2$ from MD simulations are displayed in Fig. 6, where the color code is based on σ_{von} in S-layer. In equilibrium, the defective lattice exhibits dipolar-like σ_{von} field around the dislocation (Fig. 6a), with the maximum and minimum σ_{von} located at the pentagon and heptagon rings, respectively. At small elastic strain, the weak Mo-Mo homoelemental bond is initially dissociated, resulting in inverse change in dipolar stress contour. Under intermediate level of strain, the pattern of stress contour near the dislocation cares varies from dipolar-like to 4-polar-like motif. Once a sufficient strain is applied, the atomic structure fails by direct breaking of Mo-S heteroelemental bond shared by the hexagon and heptagon on the dislocation (Fig. 6h), instead of dislocation motion. Bond and angle in perfect MoS$_2$ sustain maximum strains of around 12% and 26%, 12% and 15% under zigzag and armchair directional loads (Fig. S4), respectively, indicating that angular deformation plays a more critical role on the mechanical properties. For other dislocations with Burgers vector $\left|\vec{b}_{(1,0)}\right|$, failures by bond breakage also start with the largest polygon at the dislocation core. It is monitored that bond angles on the dislocations experience different levels of angular strain (Fig. S5), explaining their distinct mechanical properties. Such dissociation of a bond shared by hexagonal and heptagonal rings remarkably relieves the localized stress concentration on the Mo5|7 dislocation. Further straining again causes stress concentration on the as-created crack tips, where crack tip towards Mo-S-Mo angle-oriented direction is more stress concentrated, and driving crack to propagate rapidly along the armchair edge (Figs. 6b, c and i). Such brittle crack growth strongly relieves the stress field

surrounding the Mo-S-Mo angle-oriented sharp tip, but leads to high stress concentration on the S-Mo-S angle-oriented tip (Fig. 5d). Unexpectedly, brittle crack proceeds to grow towards the Mo-S-Mo angle-oriented direction, while ductile crack initiates on the S-Mo-S angle-oriented tip as the high stress-concentration reaches to critical point (Figs. 6d, k). The brittle fracture rapidly accomplishes, leading to a perfectly straight crack path (Fig. 6e). However, towards the S-Mo-S angle-orientation, ductile crack branches, with lattice reconstruction in the tip regions (Figs. 6k and l). Finally, ductile cracks proceed with deflection, leaving roughening cracking edges and atomic chains that connect the ductile crack edges (Fig. 6f). Such dual brittle and ductile fractures are also observed for other topological dislocations, excluding the armchair oriented 4|8 dislocation that shows sole brittle cracks on both sides (Fig. S7). Those reveals that the S-Mo-S angle-oriented tip plays a crucial role in load bearing and sustains large stress, although the Mo- and S-polar dislocations present inversely S-Mo-S and Mo-S-Mo oriented-angles (Fig. 6m).

4. Conclusions

In summary, MD study reveals an important previously overlooked mechanics of isolated dislocation cores in MoS_2 monolayers. Similar to the case of graphene, dislocation cores are highly stress-concentrated. Isolated dislocations with larger Burgers vectors are less energetically-favourable configurations than those with small ones, and locally wrinkle for effectively releasing the strain energy. Dislocation cores can either strengthen or weaken monolayer MoS_2, relying not only on the topology but also on the polarity of dislocations. Both atomistic simulations and theoretical studies predict the polar nature of the pre-stress field induced by a dislocation dipole. The topology and polarity of dislocations determine the maximum residual stress at the dislocation core that inversely correlates with the ultimate tensile strength. Isolated dislocation-embedded in lattice serves as the nucleation centers for cracks, through dissociation of homoelemental bonds and heteroelemental bonds at the large polygonal side on which atomic chains are removed for achieving the misfit dislocation. Brittle/ductile duality in fractures is identified in the zigzag-oriented dislocations, with

brittle and ductile cracks in Mo-S-Mo and S-Mo-S angle-oriented tips, respectively. The study provides crucial insights into the mechanical properties of synthetic MoS_2 containing ubiquitous dislocation defects and also guides the rational design of polyelemental 2D structures by dislocation engineering for practical applications.

Conflict of interest

The authors declare no competing financial interests

Supplementary data

Supporting Information Figures showing fields of relative atomic potential energies, contour plots of pre-stresses, snapshot of reconstruction of S4|4|6 dislocation, mechanical properties of pristine sheet, evolution of bond length, typical snapshots of complete rupture

Reference

[1] O.V. Yazyev, Y.P. Chen, Polycrystalline graphene and other two-dimensional materials, Nature Nanotechnology, 9 (2014) 755.

[2] L. Zhong, R.C. Bruno, K. Ethan, L. Ruitao, R. Rahul, T. Humberto, A.P. Marcos, T. Mauricio, Defect engineering of two-dimensional transition metal dichalcogenides, 2D Materials, 3 (2016) 022002.

[3] D. Akinwande, C.J. Brennan, J.S. Bunch, P. Egberts, J.R. Felts, H. Gao, R. Huang, J.-S. Kim, T. Li, Y. Li, K.M. Liechti, N. Lu, H.S. Park, E.J. Reed, P. Wang, B.I. Yakobson, T. Zhang, Y.-W. Zhang, Y. Zhou, Y. Zhu, A review on mechanics and mechanical properties of 2D materials—Graphene and beyond, Extreme Mechanics Letters, 13 (2017) 42-77.

[4] R. Xu, X. Zou, B. Liu, H.-M. Cheng, Computational design and property predictions for two-dimensional nanostructures, Materials Today, 21 (2018) 391-418.

[5] F. Ding, K. Jiao, Y. Lin, B.I. Yakobson, How Evaporating Carbon Nanotubes Retain Their Perfection?, Nano Letters, 7 (2007) 681-684.

[6] F. Ding, K. Jiao, M. Wu, B.I. Yakobson, Pseudoclimb and Dislocation Dynamics in Superplastic Nanotubes, Physical Review Letters, 98 (2007) 075503.

[7] J.H. Warner, E.R. Margine, M. Mukai, A.W. Robertson, F. Giustino, A.I. Kirkland, Dislocation-Driven Deformations in Graphene, Science, 337 (2012) 209-212.

[8] B.I. Yakobson, Mechanical relaxation and "intramolecular plasticity" in carbon nanotubes, Applied Physics Letters, 72 (1998) 918-920.

[9] X. Zou, Y. Liu, B.I. Yakobson, Predicting Dislocations and Grain Boundaries in Two-Dimensional Metal-Disulfides from the First Principles, Nano Letters, 13 (2013) 253-258.

[10] W. Zhou, X. Zou, S. Najmaei, Z. Liu, Y. Shi, J. Kong, J. Lou, P.M. Ajayan, B.I. Yakobson, J.-C. Idrobo, Intrinsic Structural Defects in Monolayer Molybdenum Disulfide, Nano Letters, 13 (2013) 2615-2622.

[11] S. Najmaei, Z. Liu, W. Zhou, X. Zou, G. Shi, S. Lei, B.I. Yakobson, J.-C. Idrobo, P.M. Ajayan, J. Lou, Vapour phase growth and grain boundary structure of molybdenum disulphide atomic layers, Nature Materials, 12 (2013) 754.

[12] A.M. van der Zande, P.Y. Huang, D.A. Chenet, T.C. Berkelbach, Y. You, G.-H. Lee, T.F. Heinz, D.R. Reichman, D.A. Muller, J.C. Hone, Grains and grain boundaries in highly crystalline monolayer molybdenum disulphide, Nature Materials, 12 (2013) 554.

[13] S. Wang, G.-D. Lee, S. Lee, E. Yoon, J.H. Warner, Detailed Atomic Reconstruction of Extended Line Defects in Monolayer MoS2, ACS Nano, 10 (2016) 5419-5430.

[14] N. Gao, Y. Guo, S. Zhou, Y. Bai, J. Zhao, Structures and Magnetic Properties of MoS2 Grain Boundaries with Antisite Defects, The Journal of Physical Chemistry C, 121 (2017) 12261-12269.

[15] O.V. Yazyev, S.G. Louie, Topological defects in graphene: Dislocations and grain boundaries, Physical Review B, 81 (2010) 195420.

[16] M.P. Ariza, C. Ventura, M. Ortiz, Force constants model for graphene from AIREBO potential, Revista Internacional de Metodos Numericos para Calculo y Diseno en Ingenieria, 27 (2011) 105-116.

[17] M.P. Ariza, R. Serrano, J.P. Mendez, M. Ortiz, Stacking faults and partial dislocations in graphene, Philosophical Magazine, 92 (2012) 2004-2021.

[18] M.P. Ariza, M. Ortiz, R. Serrano, Long-term dynamic stability of discrete dislocations in graphene at finite temperature, International Journal of Fracture, 166 (2010) 215-223.

[19] M.P. Ariza, M. Ortiz, Discrete dislocations in graphene, Journal of the Mechanics and Physics of Solids, 58 (2010) 710-734.

[20] X. Zou, M. Liu, Z. Shi, B.I. Yakobson, Environment-Controlled Dislocation Migration and Superplasticity in Monolayer MoS2, Nano Letters, 15 (2015) 3495-3500.

[21] A. Azizi, X. Zou, P. Ercius, Z. Zhang, A.L. Elías, N. Perea-López, G. Stone, M. Terrones, B.I. Yakobson, N. Alem, Dislocation motion and grain boundary migration in two-dimensional tungsten disulphide, Nature Communications, 5 (2014) 4867.

[22] Y. Han, M.-Y. Li, G.-S. Jung, M.A. Marsalis, Z. Qin, M.J. Buehler, L.-J. Li, D.A. Muller, Sub-nanometre channels embedded in two-dimensional materials, Nature Materials, 17 (2017) 129.

[23] W. Zhou, Y.-Y. Zhang, J. Chen, D. Li, J. Zhou, Z. Liu, M.F. Chisholm, S.T. Pantelides, K.P. Loh, Dislocation-driven growth of two-dimensional lateral quantum-well superlattices, Science Advances, 4 (2018).

[24] D. Taha, S.K. Mkhonta, K.R. Elder, Z.-F. Huang, Grain Boundary Structures and Collective Dynamics of Inversion Domains in Binary Two-Dimensional Materials, Physical Review Letters, 118 (2017) 255501.

[25] Z. Zhang, X. Zou, V.H. Crespi, B.I. Yakobson, Intrinsic Magnetism of Grain Boundaries in Two-Dimensional Metal Dichalcogenides, ACS Nano, 7 (2013) 10475-10481.

[26] T.H. Ly, D.J. Perello, J. Zhao, Q. Deng, H. Kim, G.H. Han, S.H. Chae, H.Y. Jeong, Y.H. Lee, Misorientation-angle-dependent electrical transport across molybdenum disulfide grain boundaries, Nature Communications, 7 (2016) 10426.

[27] Y.L. Huang, Y. Chen, W. Zhang, S.Y. Quek, C.-H. Chen, L.-J. Li, W.-T. Hsu, W.-H. Chang, Y.J. Zheng, W. Chen, A.T.S. Wee, Bandgap tunability at single-layer molybdenum disulphide grain boundaries, Nature Communications, 6 (2015) 6298.

[28] H. Nan, Z. Wang, W. Wang, Z. Liang, Y. Lu, Q. Chen, D. He, P. Tan, F. Miao, X. Wang, J. Wang, Z. Ni, Strong Photoluminescence Enhancement of MoS2 through Defect Engineering and Oxygen Bonding, ACS Nano, 8 (2014) 5738-5745.

[29] A. Splendiani, L. Sun, Y. Zhang, T. Li, J. Kim, C.-Y. Chim, G. Galli, F. Wang, Emerging Photoluminescence in Monolayer MoS2, Nano Letters, 10 (2010) 1271-1275.

[30] Y. Chenhui, D. Xi, H.L. Connie, L. Lian, Charging effect at grain boundaries of MoS 2, Nanotechnology, 29 (2018) 195704.

[31] B. Mortazavi, R. Quey, A. Ostadhossein, A. Villani, N. Moulin, A.C.T. van Duin, T. Rabczuk, Strong thermal transport along polycrystalline transition metal dichalcogenides revealed by multiscale modeling for MoS2, Applied Materials Today, 7 (2017) 67-76.

[32] J. Wu, Y. Wei, Grain misorientation and grain-boundary rotation dependent mechanical properties in polycrystalline graphene, Journal of the Mechanics and Physics of Solids, 61 (2013) 1421-1432.

[33] J. Zhang, J. Zhao, J. Lu, Intrinsic Strength and Failure Behaviors of Graphene Grain Boundaries, ACS Nano, 6 (2012) 2704-2711.

[34] Y. Wei, J. Wu, H. Yin, X. Shi, R. Yang, M. Dresselhaus, The nature of strength enhancement and weakening by pentagon–heptagon defects in graphene, Nature Materials, 11 (2012) 759.

[35] T.-H. Liu, C.-W. Pao, C.-C. Chang, Effects of dislocation densities and distributions on graphene grain boundary failure strengths from atomistic simulations, Carbon, 50 (2012) 3465-3472.

[36] T.-H. Liu, G. Gajewski, C.-W. Pao, C.-C. Chang, Structure, energy, and structural transformations of graphene grain boundaries from atomistic simulations, Carbon, 49 (2011) 2306-2317.

[37] R. Grantab, V.B. Shenoy, R.S. Ruoff, Anomalous Strength Characteristics of Tilt Grain Boundaries in Graphene, Science, 330 (2010) 946-948.

[38] Z. Song, V.I. Artyukhov, B.I. Yakobson, Z. Xu, Pseudo Hall–Petch Strength Reduction in Polycrystalline Graphene, Nano Letters, 13 (2013) 1829-1833.

[39] J. Wu, P. Cao, Z. Zhang, F. Ning, S.-s. Zheng, J. He, Z. Zhang, Grain-Size-Controlled Mechanical Properties of Polycrystalline Monolayer MoS2, Nano Letters, 18 (2018) 1543-1552.

[40] S. Wang, Z. Qin, G.S. Jung, F.J. Martin-Martinez, K. Zhang, M.J. Buehler, J.H. Warner, Atomically Sharp Crack Tips in Monolayer MoS2 and Their Enhanced Toughness by Vacancy Defects, ACS Nano, 10 (2016) 9831-9839.

[41] X. Si, C. Guoxin, Molecular dynamics simulations of mechanical properties of monolayer MoS 2, Nanotechnology, 26 (2015) 185705.

[42] J. Wu, G. Nie, J. Xu, J. He, Q. Xu, Z. Zhang, Structural instability and mechanical properties of MoS2 toroidal nanostructures, Physical Chemistry Chemical Physics, 17 (2015) 32425-32435.

[43] B. Radisavljevic, A. Radenovic, J. Brivio, V. Giacometti, A. Kis, Single-layer MoS2 transistors, Nature Nanotechnology, 6 (2011) 147.

[44] Y. Liu, B.I. Yakobson, Cones, Pringles, and Grain Boundary Landscapes in Graphene Topology, Nano Letters, 10 (2010) 2178-2183.

[45] Z. Song, Z. Xu, Topological Defects in Two-Dimensional Crystals: The Stress Buildup and Accumulation, Journal of Applied Mechanics, 81 (2014) 091004-091005.

[46] B.I. Yakobson, F. Ding, Observational Geology of Graphene, at the Nanoscale, ACS Nano, 5 (2011) 1569-1574.

[47] X. Si, C. Guoxin, Bending response of single layer MoS 2, Nanotechnology, 27 (2016) 105701.

[48] T. Zhang, X. Li, H. Gao, Defects controlled wrinkling and topological design in graphene, Journal of the Mechanics and Physics of Solids, 67 (2014) 2-13.

[49] Z.G. Yu, Y.-W. Zhang, B.I. Yakobson, An Anomalous Formation Pathway for Dislocation-Sulfur Vacancy Complexes in Polycrystalline Monolayer MoS2, Nano Letters, 15 (2015) 6855-6861.
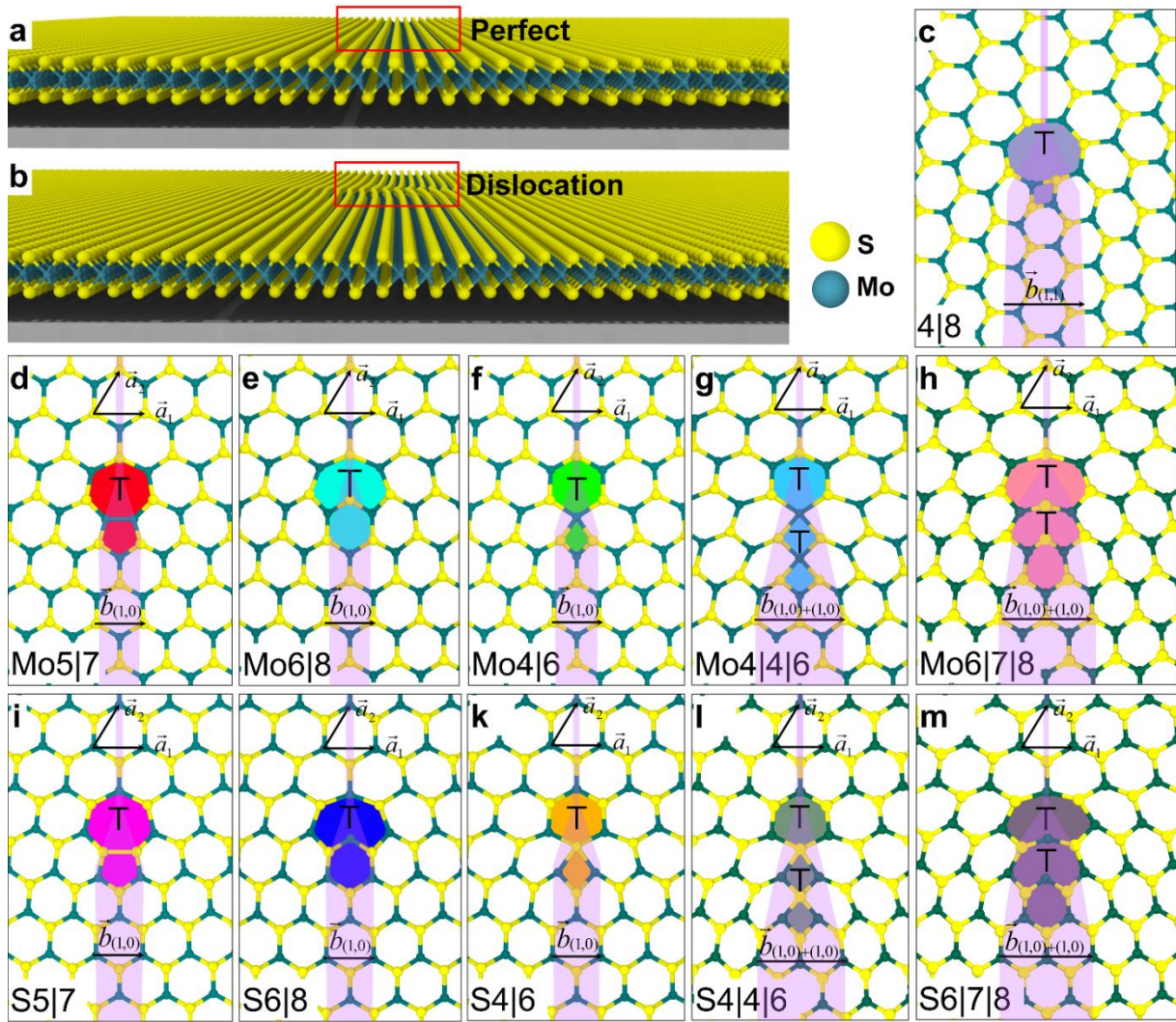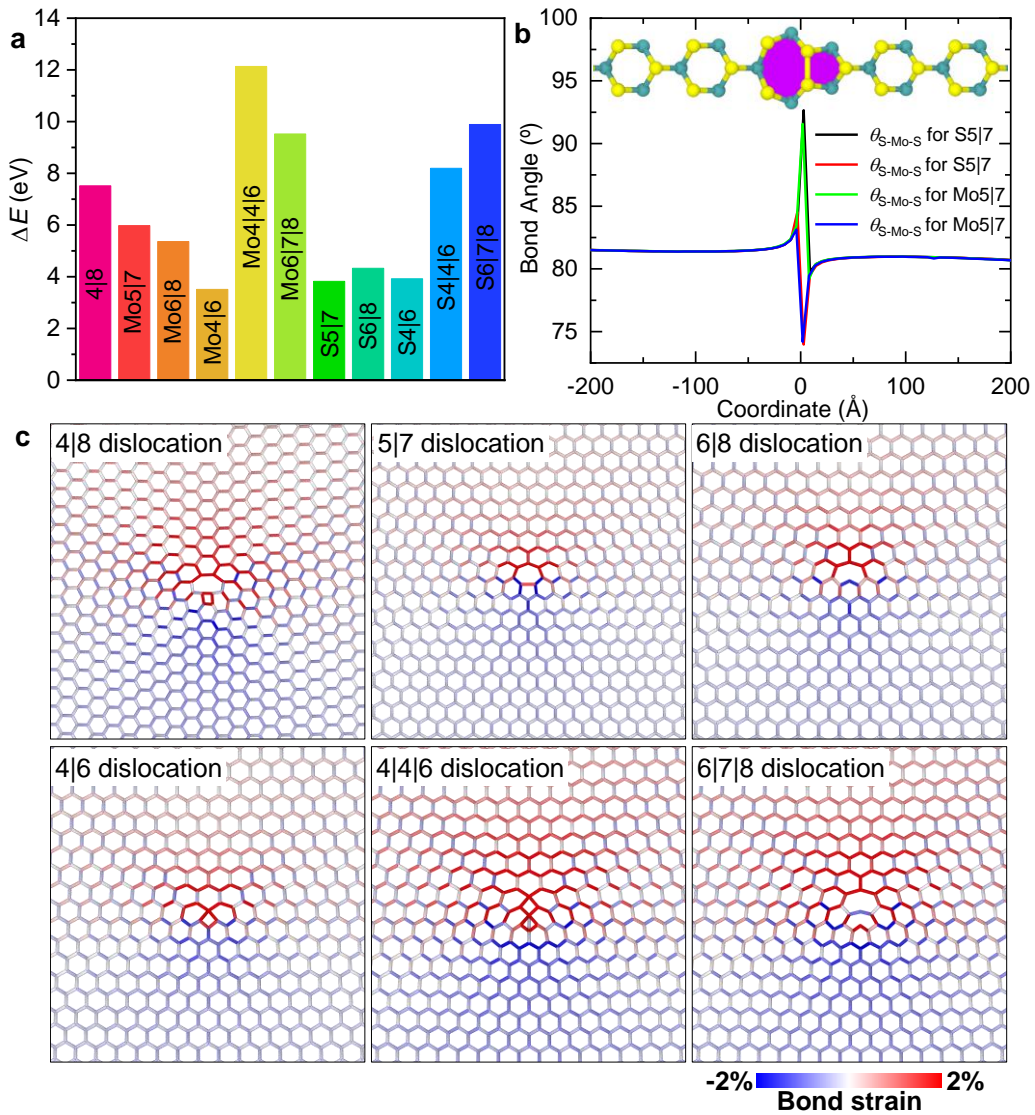
Fig. 1 Dislocation cores in monolayer MoS$_2$. (**a**) and (**b**) Perspective view of defect-free and an isolated dislocation-embedded MoS$_2$ lattice. Atomic structures of (**c**) 4|8 dislocation core with Burgers vector $\left|\vec{b}_{(1,1)}\right|$, (**d**)-(**f**) Mo-oriented polar Mo5|7, Mo6|8 and Mo4|6 dislocation cores with the same Burgers vector $\left|\vec{b}_{(1,0)}\right|$, (**g**) and (**h**) Mo-oriented polar Mo4|4|6 and Mo6|7|8 dislocation cores with Burgers vector $\left|\vec{b}_{(1,0)+(0,1)}\right|$, (**i**)-(**k**) S-oriented polar S5|7, S6|8 and S4|6 dislocation cores with Burgers vector $\left|\vec{b}_{(1,0)}\right|$ and (**l**) and (**m**) S-oriented polar S4|4|6 and S6|7|8 dislocation cores with Burgers vector $\left|\vec{b}_{(1,0)+(0,1)}\right|$, respectively.

Fig. 2 Energetics and bond characteristics in isolated dislocation-contained MoS_2 monolayers. (**a**) Potential energies of the 11 types of dislocation cores in MoS_2 monolayers with respect to the bulk counterpart, respectively. (**b**) Bond angle distribution of the middle nanoribbons containing Mo5|7 and S5|7 dislocation cores in MoS_2 monolayer. Inset presents the typical atomic structure of S5|7 dislocation-contained MoS_2 nanoribbon. (**c**) Fields of bond strain surrounding isolated 4|8, 5|7, 6|8, 4|6, 4|4|6 and 6|7|8 dislocation cores in MoS_2 monolayer with respect to the bulk counterpart, respectively. Bonds are colored on the basis of bond strain in equilibrated MoS_2 monolayers containing an isolated dislocation.
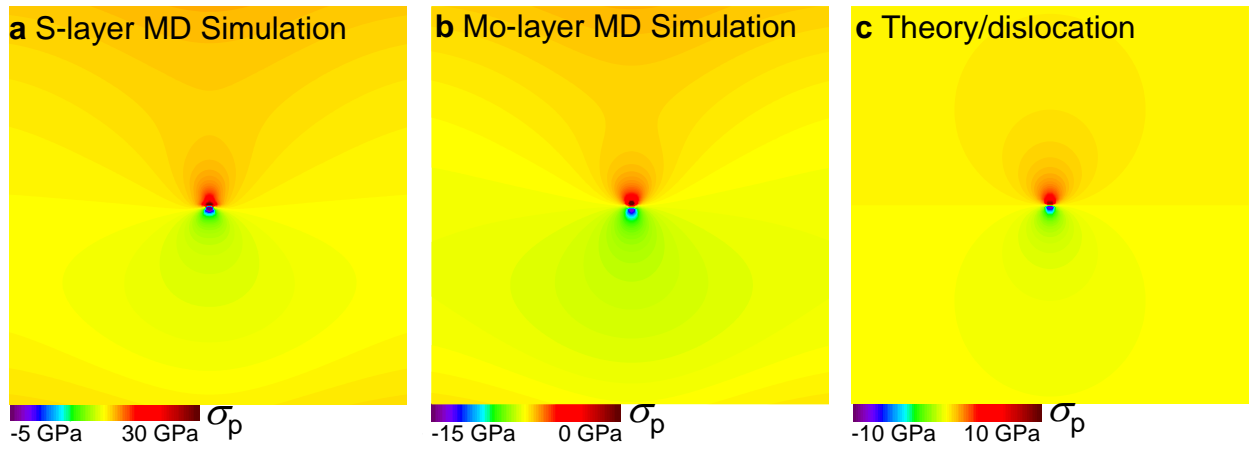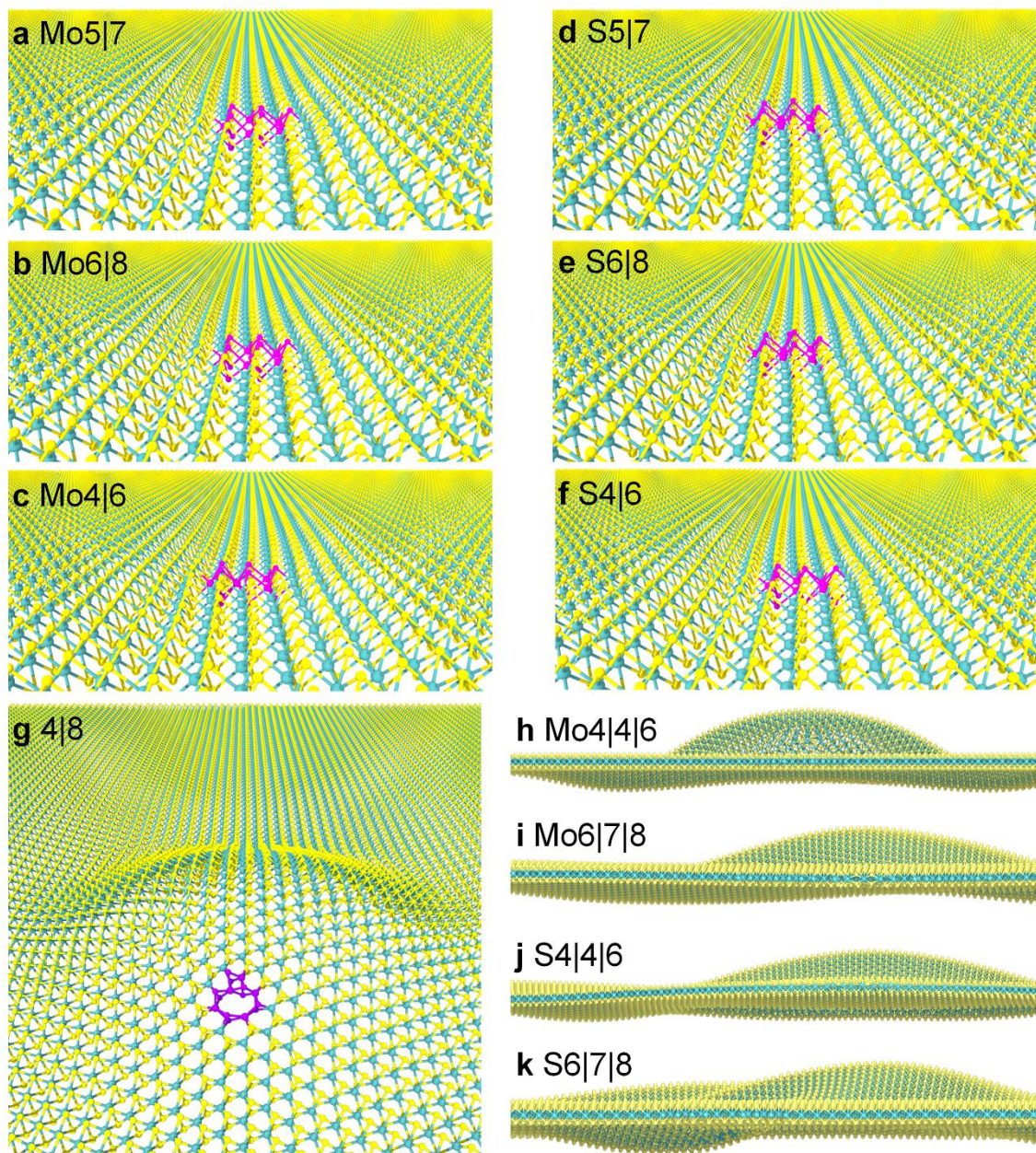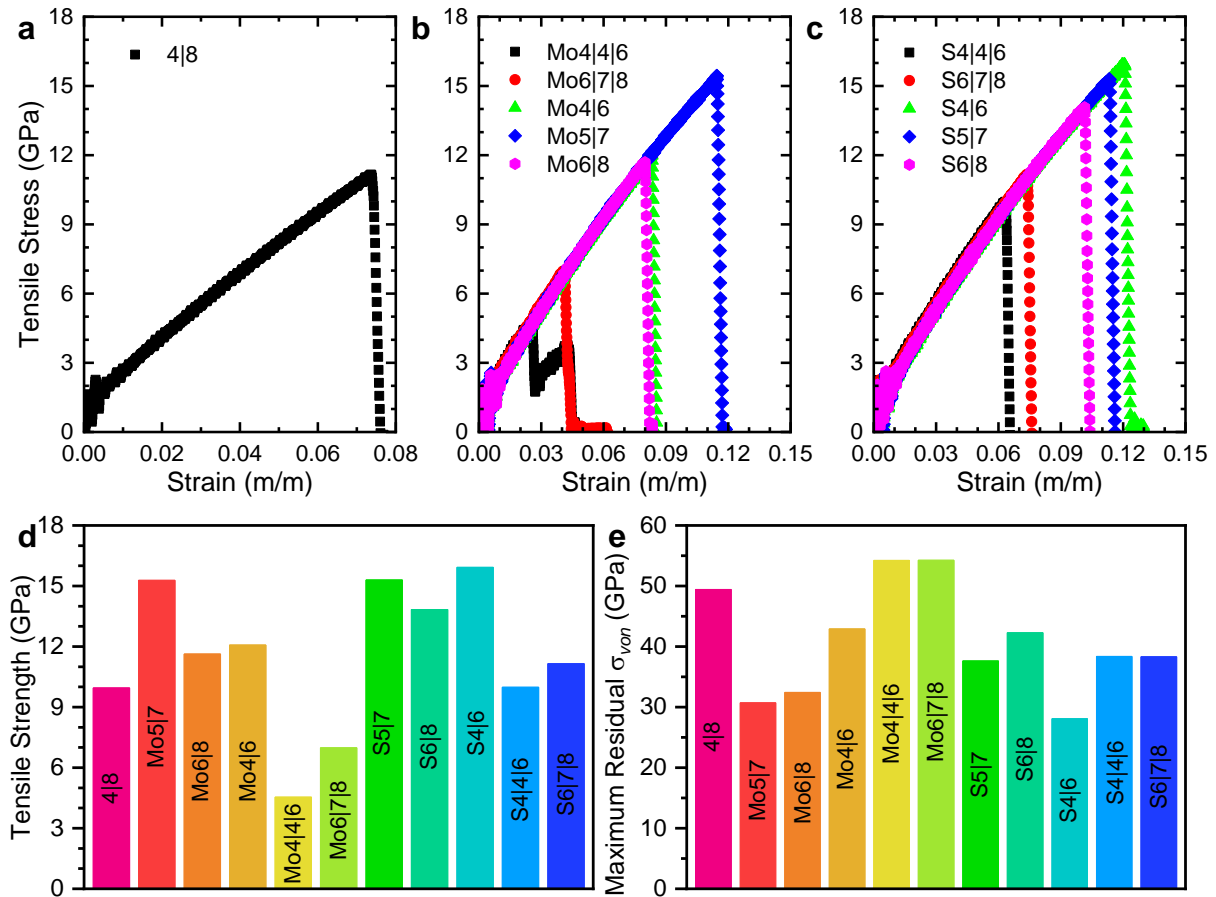
Fig. 3 Pre-stresses in isolated dislocation-contained MoS$_2$ monolayers. (**a**) and (**b**) Typical fields of the principal stress $\sigma_{\mathrm{p}} = \frac{1}{2}\left(\sigma_{xx} + \sigma_{yy}\right)$ from MD simulations for sandwich central Mo- and S-layers in single Mo5|7 dislocation-contained MoS$_2$ monolayer, respectively. (**c**) Predicted field of principal stress σ_{p} from 2D elastic theory for comparison.

Fig. 4 Out-of-plane characteristics of MoS_2 monolayers induced by isolated dislocation cores. (**a**)-(**c**) Perspective views of planar structures of single Mo5|7, Mo6|8 and Mo4|6 dislocation-contained MoS_2 monolayers, respectively. (**d**)-(**f**) Perspective views of planar structures of single S5|7, S6|8 and S4|6 dislocation-contained MoS_2 monolayers, respectively. (**g**) Perspective view of wrinkle in isolated 4|8 dislocation-embedded MoS_2 monolayer. (**h**)-(**k**) Side-views of isolated dislocations in MoS_2 monolayers are purple-highlighted for enhanced visibility.

Fig. 5 Mechanical properties of isolated dislocation-contained MoS_2 monolayers. (**a**)-(**c**) Mechanical stress-strain curves of 11 different dislocation-contained MoS_2 subjected to uniaxial tension perpendicular to the dislocations, respectively. (**d**) Ultimate tensile strength of the 11 different dislocation-embedded MoS_2 monolayers. (**e**) Maximum residual stress σ_{von} in the 11 dislocation-contained MoS_2 monolayers.
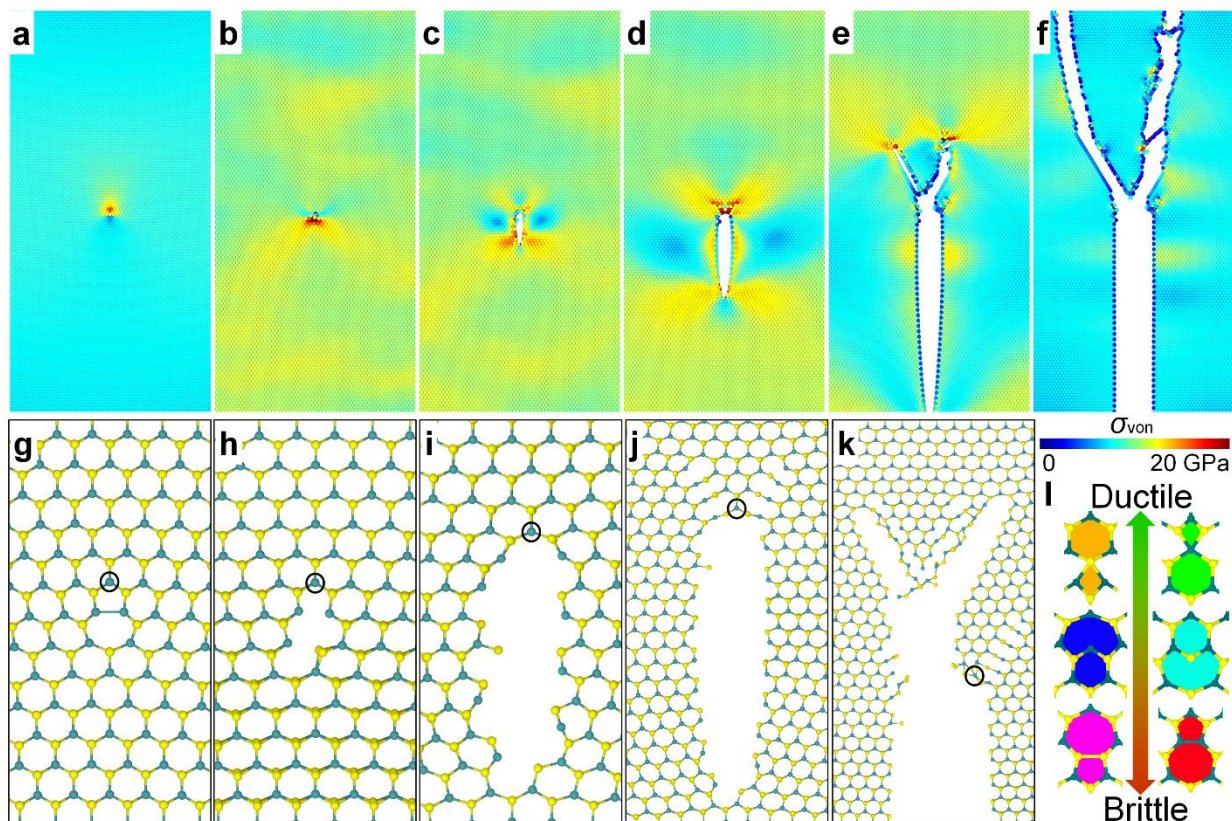
Fig. 6 Representative fracturing characteristics in an isolated dislocation-contained MoS$_2$ monolayer. (**a**)-(**k**) Snapshots illustrating the typical fracture process of an isolated Mo5|7 dislocation-contained MoS$_2$ under uniaxial straining along the horizontal direction. Atoms in MoS$_2$ monolayer are colored based on their values of *von Mises* stress σ_{von}. (**l**) Illustration of dual brittle/ductile fractures in the polar dislocation (Mo4|6, Mo6|8, Mo5|7, S4|6, S6|8 and S5|7) sides. Towards Mo-S-Mo angular orientation in dislocation cores, brittle crack occurs, whereas towards S-Mo-S angular orientation in dislocation cores, ductile fracture is identified.

Graphical abstract